

# Multitarget Bistatic MIMO RADAR

Nadeem Dar and Athanassios Manikas

Department of Electrical and Electronic Engineering

Imperial College London

**Abstract**—This paper is concerned with the investigation of the bistatic MIMO radar for estimating various multitarget parameters of interest in the presence of clutter and noise. The parameters of interest include Direction of Departure (DOD), Direction of Arrival (DOA), range and velocity and a novel algorithm is proposed for estimating these target parameters based on the concepts of the "array manifold" and "manifold extenders". The performance of the proposed algorithm is evaluated using Monte Carlo simulation studies.

**Index Terms**—Bistatic MIMO Radar, Direction of Arrival, Direction of Departure, Array Manifold, Manifold Extenders

## NOTATIONS

$a, A$	Scalar
$\underline{a}, \underline{A}$	Column Vector
$A$	Matrix
$(\cdot)^T, (\cdot)^H$	Transpose, Hermitian transpose
$(\cdot)^{\#}$	Pseudo-inverse
$(\cdot)^*$	Conjugate
$E\{\cdot\}$	Expectation operator
$\otimes$	Kronecker product
$\odot$	Hadamard product
$\circledast$	Convolution
$\forall$	"for all"
$\underline{1}_N$	Column vector of $N$ ones
$\underline{0}_N$	Column vector of $N$ zeros
$I_N$	$N \times N$ Identity matrix
$R, C$	Set of real & complex numbers
$\underline{\text{col}}_{\ell}$	$\ell$ -th column of a matrix

## I. INTRODUCTION

Modern radars operate in the presence of objects/targets, clutter, noise and interferences [1]. The main objectives of a radar are to detect the presence of targets and estimate their parameters, especially when targets are located close together in space. Once the presence of a target is detected in clutter, then the aims are:

- to accurately estimate various target parameters, such as range, direction and velocity, and
- to solve the targets' "classification" problem, i.e. identify the type of target by getting its "electronics signature".

The simplest radar architecture is the "monostatic" [2] where the Tx and Rx antennas are "collocated", and thus the DOD (Direction of Departure) from the radar's Tx to the target is identical to the DOA (Direction of Arrival) from the target to the radar's Rx. Some popular examples of DOA estimation for monostatic MIMO radar are the Least Square (LS), Capon and Amplitude and Phase Estimation (APES) MIMO algorithms [3].

This paper is concerned with "bistatic" radar where there is some considerable distance between the radar's Tx and Rx. Consequently, the DOA is different from the DOD. Bistatic radars introduce several technical complications but there are many significant advantages relative to monostatic radar architectures. For instance, bistatic radar can handle stealthy targets while "jamming" is very difficult. The most powerful and modern monostatic/bistatic radar is the MIMO radar which employs antenna arrays of known geometries at both the Tx and Rx sides. As the title of the paper suggests, this work is concerned with bistatic MIMO radar with emphasis given to DOA and DOD estimation. Existing DOA-DOD estimation algorithms in bistatic MIMO radar have been reported in [4]–[7].

In [4], a joint DOA and DOD estimation algorithm is proposed for bistatic MIMO radar based on a polynomial root-finding subspace method. The main drawback of [4] is that the proposed algorithm is restricted to bistatic MIMO where both Tx and Rx arrays are uniform linear arrays.

In [5], a two-dimensional DOA and DOD estimation is proposed based on parallel factor (PARAFAC) analysis instead of Eigenvector decomposition. The paper claims the computational efficiency using tensor processing, but no computational complexity comparison with any conventional method is presented.

In [6], a DOA-DOD and Range estimation is presented for Frequency Diverse Array FDA-MIMO radar. This is a specific form of MIMO radar which suffers from the "ambiguity problem" where a single target appears to have many ranges and many DOD. Thus, [6] is mainly focused on resolving the ambiguity problem while it also assumes ULA for both Tx and Rx arrays.

In [7], the time synchronization is proposed between the Tx and Rx sites. First, it estimates the bistatic range through matched filtering and non-linear least squares (NLS) optimisation. Then the DOA and DOD are calculated using the known bistatic geometry i.e., the bistatic baseline, Tx, and Rx array locations. Finally, the synchronization offset is calculated through the estimated/calculated parameters variance. This calculation is only possible in the presence of a single target, and the system requires a high SNR to operate reasonably.

As stated before, in this paper DOA and DOD are the primary parameters to be estimated based on the concept of "extended manifolds" which are functions of the array manifold. For plane-wave propagation, the array manifold is a vector function of the target direction, array geometry and carrier frequency. Array manifolds (or simply manifolds) are mathematical objects such as "curves", "surfaces" etc. (i.e., non-linear subspaces). These manifolds have been analysed in

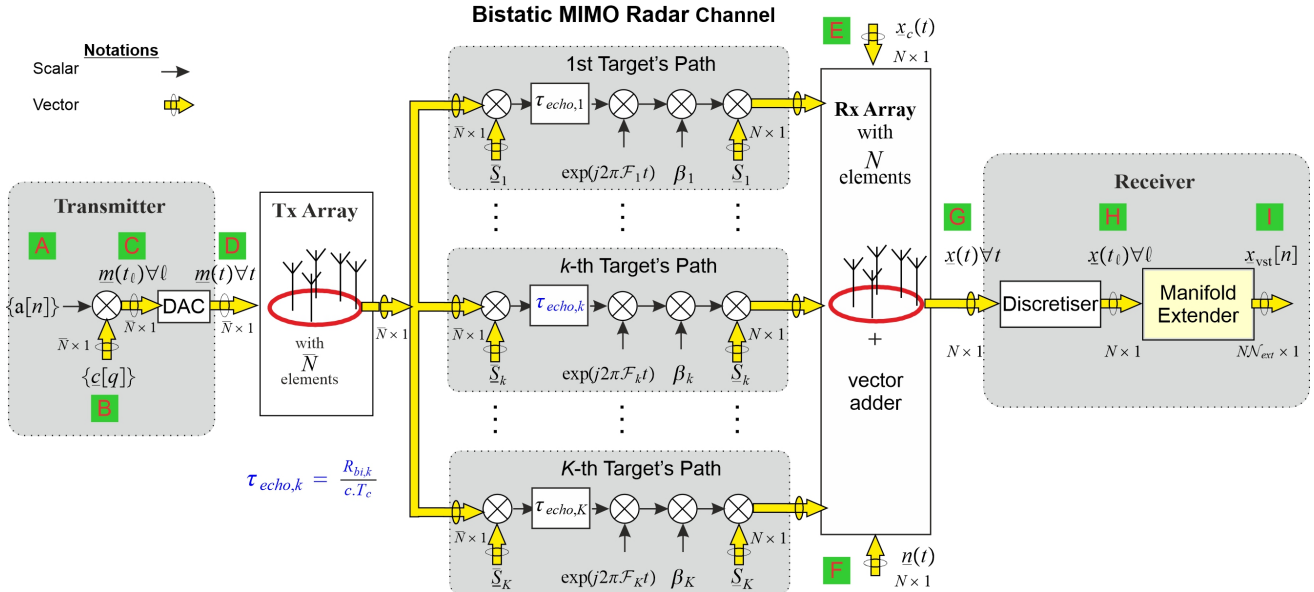


Fig. 1: Multi-Target MIMO Radar

[8] and their shapes and parameters are directly connected to the accuracy, resolution, and detection capabilities of the array.

These days more radar system and target parameters may be added to the array manifold beyond the array geometry, the target direction and the carrier frequency. These new manifolds with additional parameters of interest are known as extended manifolds [9] to separate them from the standard manifold which for convenience are also known as “spatial” array manifolds. Such additional parameters may be polarisation, Doppler, delay, PN-codes, and multi-carriers, etc. Every time a new system parameter is added, instead of having a complex analysis like the one presented in [8], the aim is to express the extended manifold vector as a function of the spatial manifold vector and make a direct connection to the properties and capabilities between the new manifold and the original spatial manifold.

In this paper, the "manifold extender" will be used by starting with the Rx spatial array manifold and then forming the Rx's extended manifold by adding the following three new but unknown parameters:

- the target's range-bin,
- Doppler frequency (for moving targets),
- The DOD from the Tx to the target.

This paper builds on the DOA and DOD estimation proposed in [10] for a MIMO communication system. It explores the virtual array concept (a form of extended array manifold [9], [11]) to extend the system's observation space from  $N$  (number of Rx antennas) to  $N\bar{N}$  (i.e. the product of Rx antennas  $N$  and the Tx antennas  $\bar{N}$ ), hence enabling to detect and process more targets than Rx antenna elements with greater resolution capabilities<sup>1</sup>.

In summary, this paper builds upon the ideas put forth in previous works, including those by [9]–[12], and extends the concept to Multitarget Bistatic MIMO radar. The paper is structured as follows: In Section 2, the generation of the Tx baseband signal of the proposed system is presented. In Section 3, the MIMO multitarget channel model that will be used in this paper is discussed. Section 4 is concerned with the modelling of the received array vector signal. Section 5 focuses on the proposed parameter estimation algorithms, while Section 6 details the computer simulation environments and results. The paper is concluded in Section 7.

## II. Tx SIGNAL MODELLING

FIGURE 1 conceptually illustrates a bistatic MIMO radar architecture with the yellow arrow representing vectors of parallel signals. At Point-A of the transmitter (Tx), a sequence of  $N_s$  symbols  $\{a[n] \in \{\pm 1\}, \forall n = 1, 2, \dots, N_s\}$  is used with pulse duration  $T_p$ . The Tx uses an antenna array of  $\bar{N}$  antennas and the sequence  $\{a[n] \in \{\pm 1\}\}$  is copied to all the  $\bar{N}$  RF units. Then this sequence is spread over a larger bandwidth by using a vector of  $\bar{N}$  PN-codes (one PN-code per Tx-antenna) as shown at Point-B. All these PN-codes have length  $\mathcal{N}_c$  and chip period  $T_c$  with

$$\mathcal{N}_c T_c = T_p \quad (1)$$

The radar's PRI (Pulse Repetition Interval) is assumed having  $N_p$  uncompressed range bins or, equivalently,  $N_p \mathcal{N}_c$  compressed range bins. That is

$$\text{PRI} = N_p T_p \quad (2)$$

$$= N_p \mathcal{N}_c T_c \quad (3)$$

Figure 2 illustrates the above time frame structure of the radar, considering also that the CPI (coherent processing

<sup>1</sup>The concept of the extended array manifold has been also used in [12] for monostatic MIMO radar and showed that the extended array manifold algorithms outperformed the conventional algorithms/processing with respect to RMSE criterion.

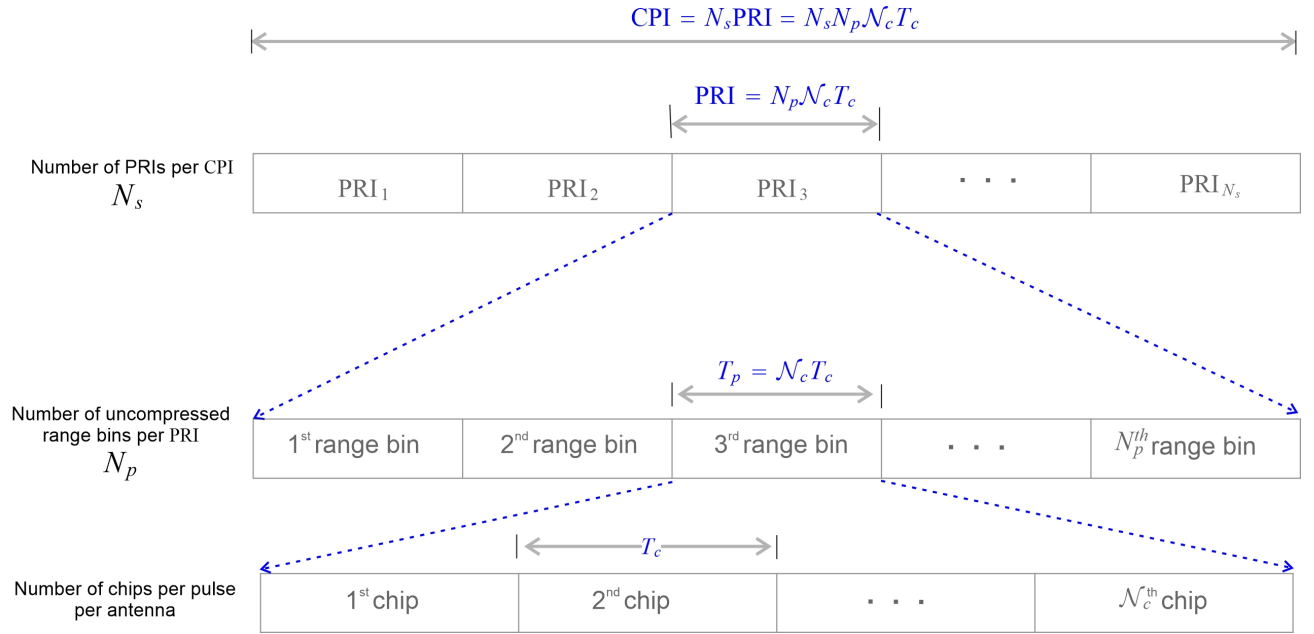


Fig. 2: Baseband Tx Signal Generation

interval) over which the radar will estimate the various target parameters has a duration equal to  $N_s \text{PRI}$ . That is:

$$\text{CPI} = N_s \text{PRI} = N_s N_p N_c T_c \quad (4)$$

$$= N_s N_p N_c T_c \quad (5)$$

The number of data symbols generated at Point-C of Figure 1 over one CPI can be modelled by the following matrix  $\mathbb{M}$ :

$$\mathbb{M} \triangleq [\underline{m}_1, \underline{m}_2, \dots, \underline{m}_{N_s N_p N_c}] \quad (6)$$

$$= \underline{a}^T \otimes \underbrace{[\mathbb{C}, \mathbb{O}_{\bar{N} \times (N_p N_c - N_c)}]}_{\triangleq \mathbb{C}_{ex}^T \in \mathcal{R}^{\bar{N} \times N_p N_c}} \in \mathcal{R}^{\bar{N} \times N_s N_p N_c} \quad (7)$$

where the data symbols vector  $\underline{a}$  is defined as

$$\underline{a} \triangleq [a[1], a[2], \dots, a[N_s]]^T \in \mathcal{R}^{N_s \times 1} \quad (8)$$

and the PN-codes matrix has been extended with zeros until the end of each PRI, i.e.  $N_p N_c - N_c$  columns of  $\bar{N}$  zeros

$$\begin{aligned} \mathbb{C}_{ex}^T &= [\underline{c}[1], \underline{c}[2], \dots, \underline{c}[q], \dots, \underline{c}[N_p N_c]] \in \mathcal{R}^{\bar{N} \times N_p N_c} \\ &= \underbrace{\begin{bmatrix} \alpha_1[1], & \alpha_1[2], & \dots & \alpha_1[N_c], & 0, & 0, & \dots & 0 \\ \alpha_2[1], & \alpha_2[2], & \dots & \alpha_2[N_c], & 0, & 0, & \dots & 0 \\ \vdots & \vdots & & \vdots & \vdots & \vdots & & \vdots \\ \alpha_{\bar{N}}[1], & \alpha_{\bar{N}}[2], & \dots & \alpha_{\bar{N}}[N_c], & 0, & 0, & \dots & 0 \end{bmatrix}}_{\triangleq \mathbb{C}^T} \underbrace{N_p N_c - N_c}_{\text{columns of } \bar{N} \text{ zeros}} \end{aligned} \quad (9)$$

As shown at Point-B of Figure 1, the  $q$ -th column of the  $\mathbb{C}_{ex}^T$  above matrix is the vector  $\underline{c}[q]$ . The  $\ell$ -th column<sup>2</sup> of the matrix  $\mathbb{M}$  (i.e.  $m_\ell$ ) representing the symbols that appear at Point-C during the chip interval  $\ell T_c$ . It is important to point out that the PN-code matrix  $\mathbb{C}$  has a covariance matrix approximately

equals to an identity matrix (almost orthogonal PN-codes). That is:

$$\mathbb{R}_{CC} = \frac{1}{N_c} \mathbb{C}^T \mathbb{C} \approx \mathbb{I}_{\bar{N}} \in \mathcal{R}^{\bar{N} \times \bar{N}} \quad (10)$$

Then it is easy to see (using Equation 7) that the covariance matrix for the data matrix  $M$  is

$$\mathbb{R}_{MM} = \frac{1}{N_c N_s} \mathbb{M} \mathbb{M}^T \approx \mathbb{I}_{\bar{N}} \in \mathcal{R}^{\bar{N} \times \bar{N}} \quad (11)$$

At Point-D in Figure 1, after the DAC (digital to analogue converter) block, the analogue baseband transmitted vector signal is represented as follows:

$$\underline{m}(t) = [m_1(t), m_2(t), \dots, m_{\bar{N}}(t)]^T \quad (12)$$

### III. RADAR CHANNEL MODEL

The wireless MIMO channel is modelled as shown in Figure 1 between Points-D and G. It considers a bistatic MIMO pulse radar operating in the presence of  $K$  moving targets. The geometry of the  $k$ -th moving target is shown in Figure 3 having velocity  $v_k$  at a bistatic range  $R_{bi,k}$ .

The vector-signal at the output Point-D in Figure 1 is transformed by the Tx antenna array to a vector of  $\bar{N}$  electromagnetic waves (one per antenna) which will propagate through our 3D physical space. The various "displacements" of these electromagnetic waves at the Tx antennas are a function of

- the Tx-array geometry, and
- their direction of propagation  $(\bar{\theta}_k, \bar{\phi}_k)$ , where  $\bar{\theta}_k$  represents azimuth and  $\bar{\phi}_k$  elevation angles.

These electromagnetic "displacements" for the  $k$ -th target's direction  $(\bar{\theta}_k, \bar{\phi}_k)$  are modelled by the Tx manifold vector:

$$\begin{aligned} \underline{S}_k &\triangleq \underline{S}(\bar{\theta}_k, \bar{\phi}_k) \in \mathcal{C}^{\bar{N} \times 1} \\ &= \exp(+j[\bar{x}_x, \bar{x}_y, \bar{x}_z] \underline{k}(\bar{\theta}_k, \bar{\phi}_k)) \end{aligned} \quad (13)$$

<sup>2</sup>Note that  $\ell$  is an integer taking values 1, 2, ...,  $N_s N_p N_c$ .

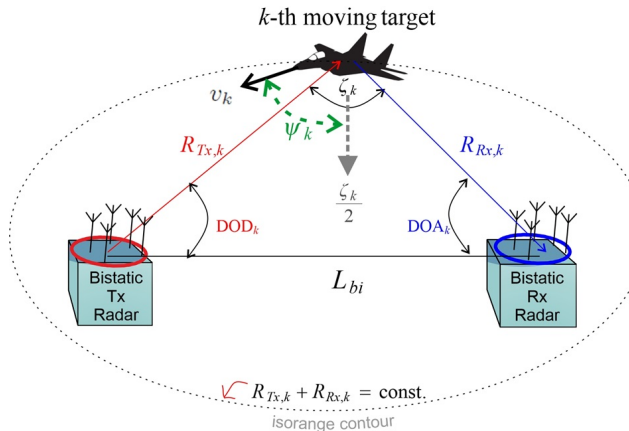


Fig. 3: Bistatic Radar's Target

where

$$[\bar{r}_x, \bar{r}_y, \bar{r}_z] = \text{Tx antenna array geometry} \quad (14)$$

$$\underline{k}(\bar{\theta}_k, \bar{\phi}_k) = \frac{2\pi}{\lambda} \underline{u}(\bar{\theta}_k, \bar{\phi}_k) \text{ is wavenumber vector} \quad (15)$$

with  $\underline{u}(\bar{\theta}_k, \bar{\phi}_k)$  being a unity norm vector pointing towards the direction of departure, i.e.

$$\underline{u}(\bar{\theta}_k, \bar{\phi}_k) = \begin{bmatrix} \cos \bar{\theta}_k \cos \bar{\phi}_k \\ \sin \bar{\theta}_k \cos \bar{\phi}_k \\ \sin \bar{\phi}_k \end{bmatrix} \quad (16)$$

The transmitted electromagnetic waves will be reflected by the  $k$ -th target and the echo will be received by the radar's Rx antenna array after a propagation time

$$\tau_{echo,k} = \frac{R_{Tx,k} + R_{Rx,k}}{c}, \forall k, \quad (17)$$

$$d_k = \left\lfloor \frac{\tau_{echo,k}}{T_c} \right\rfloor \quad (18)$$

where  $c$  is the speed of light. Figure 1 shows the delay  $\tau_{echo,k}$ , the path gain  $\beta_k$  and the effects of the target's Doppler frequency  $\mathcal{F}_k$ . Note that the parameter  $\beta_k$  in Figure 1 is modelled as follow:

$$\beta_k = |\beta_k| \exp(j\psi_k) \quad (19)$$

where

$$|\beta_k| = \sqrt{\frac{G_{Tx}G_{Rx}}{(4\pi)^3}} \cdot \left( \frac{\lambda}{R_{Tx}R_{Rx}} \right) \cdot \sqrt{\text{RCS}_k} \quad (20)$$

$$\underline{\beta}_k = \exp\left(-j2\pi F_c \frac{R_{bi,k}}{c}\right) \exp(j\psi_k) \exp(j2\pi \mathcal{F}_k t) \quad (21)$$

and  $\psi_k$  is random phase. Thus the parameter  $\beta_k$  of the  $k$ -th target is a function of:

- the target's radar cross section ( $\text{RCS}_k$ ),
- the antenna gains of the Tx and Rx, i.e.  $G_{Tx}$  and  $G_{Rx}$  respectively,
- the Tx to target range  $R_{Tx,k}$  and target to Rx range  $R_{Rx,k}$ .

The channel model also considers targets' movement and resulting Doppler shift on the Tx carrier frequency. In Figure 1 the Doppler shift of the  $k$ -th moving target is represented by the term  $\exp(j2\pi \mathcal{F}_k t)$ . For the bistatic geometry of Figure 3, this Doppler shift is given as follows [1]:

$$F_k = \frac{2v_k}{\lambda} \cos \psi_{bi,k} \cos \frac{\zeta_k}{2} \quad (22)$$

where the subscript  $k$  signifies the  $k$ -th target,  $v_k$  denotes its velocity,  $\zeta_k$  is the angle between incident and reflected wave, and  $\psi_{bi,k}$  represents the angle between the discontinuous  $\frac{\zeta_k}{2}$  and the direction of movement.

In a similar fashion, for the  $k$ -th target, the various "displacements" of the electromagnetic waves arriving at the Rx antenna array with direction of arrival  $\theta_k, \phi_k$  is modelled by the Rx manifold vector:

$$\underline{S}_k \triangleq \underline{S}(\theta_k, \phi_k) \in \mathcal{C}^{N \times 1} \quad (23)$$

$$= \exp(-j[r_x, r_y, r_z] \underline{k}(\theta_k, \phi_k)) \quad (24)$$

where the matrix  $[r_x, r_y, r_z]^T$  denotes the Cartesian coordinates of the Rx antenna array elements and  $\underline{k}(\theta_k, \phi_k)$  is the wavelength vector corresponding to the Direction of Arrival (DOA).

Based on the above, the impulse response ( $IR$ ) of a MIMO radar channel can be summarised using the following equation:

$$IR = \sum_{k=1}^K \beta_k \exp(j2\pi F_k t) \underline{S}_k \underline{S}_k^H \underline{\delta}(t - \tau_{echo,k}) \quad (25)$$

#### IV. RADAR RECEIVER BASED ON "MANIFOLD EXTENDER"

At Point-G of Figure 1, based on the radar's channel modelling presented in Section III, the analogue received vector-signal  $\underline{x}(t) \in \mathcal{C}^{N \times 1}$  at the output of the Rx antenna array can be written as:

$$\underline{x}(t) = [x_1(t), x_2(t), \dots, x_N(t)]^T \in \mathcal{C}^{N \times 1} \quad (26)$$

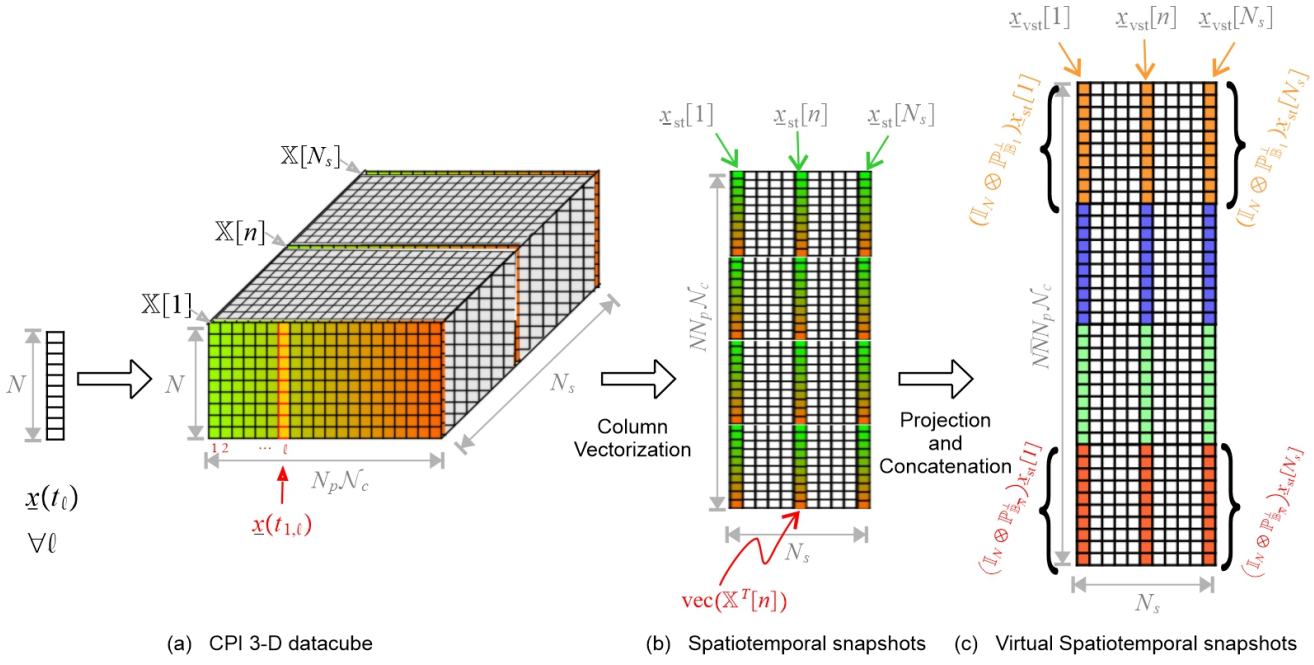
$$= \sum_{k=1}^K \underbrace{\sqrt{P_{Tx}} \beta_k \exp(j2\pi \mathcal{F}_k t) \underline{S}_k^H}_{\text{scalar signal (echo) from the } k\text{-th target}} \underline{m}(t - \tau_{echo,k}) \underline{S}_k + \underline{x}_c(t) + \underline{n}(t) \quad (27)$$

where  $\underline{x}_c(t)$  represents the "clutter" effects and  $\underline{n}(t)$  is the complex additive white Gaussian noise (AWGN) of  $\mathcal{CN}(0, \sigma_n^2 I_N)$ , i.e. of zero mean and covariance matrix  $\mathbb{R}_{nn} = \sigma_n^2 I_N$ . Remember that the subscript  $k$  refers to the  $k$ -th target and a bar on top of a symbol represents a Tx parameter.

The analogue vector-signal  $\underline{x}(t)$  at Point-G of Figure 1 is then digitised to produce at Point-H the  $\ell$ -th snapshot vector  $\underline{x}(t_\ell), \forall \ell = 1, 2, \dots$ , which is represented as:

$$\underline{x}(t_\ell) = [x_1(t_\ell), x_2(t_\ell), \dots, x_N(t_\ell)]^T \in \mathcal{C}^{N \times 1} \quad (28)$$

These snapshots,  $\forall \ell$ , at Point-H are then driven to a suitable "manifold extender" block which is going to be employed by the proposed novel algorithm for estimating both DOA and DOD of all targets.

Fig. 4: MIMO Radar Rx 3-D Data Cube  $\mathbb{X}$  for One CPI and Extended Snapshots Formation

### A. Manifold Extender

The manifold extender involves a complex mapping of spatial manifold to extended manifold using additional system parameters. In this paper these additional parameters are the DOD, radar's range bins, the PN-code matrix  $\mathbb{C}$  and the Doppler frequency. That is

$$\underline{S}_k: \text{is a function of DOA}_k, F_c, c \text{ and array geometry} \quad (29)$$

$$\underline{h}_k: \text{is a function of } \underline{S}_k \text{ (see Equ. 29) plus DOD}_k, \mathbb{C}, \ell_k, \mathcal{F}_k \quad (30)$$

This implies that:

- at Point-H of Figure 1:  $\underline{x}(t_\ell) \in \mathcal{C}^{N \times 1}$ , with

$$\underline{x}(t_\ell) = \left( \sum_{k=1}^K \text{function of } \underline{S}_k \right) + \text{clutter} + \text{noise} \quad (31)$$

- at Point-I of Figure 1:  $\underline{x}_{\text{vst}}[n] \in \mathcal{C}^{N N_{\text{ext}} \times 1}$ , with

$$\underline{x}_{\text{vst}}[n] = \left( \sum_{k=1}^K \text{function of } \underline{h}_k \right) + \text{clutter} + \text{noise} \quad (32)$$

where

$$N_{\text{ext}} = \bar{N} N_p \mathcal{N}_c$$

To go from Equation 31 to Equation 32 the input data at Point-H should be re-arranged in a suitable way so that Equation 29 is transformed to Equation 30. This re-arrangement of data is shown in Figure 4 and is described as follows:

- The snapshot at time instant  $t_\ell$  is denoted so far by  $\underline{x}(t_\ell)$  where  $\ell$  takes values  $1, 2, \dots, N_s N_p \mathcal{N}_c$  representing

the whole CPI. However, for every PRI we collect its  $N_p \mathcal{N}_c$  snapshot vectors. To reflect this collection of snapshots to a specific PRI, the notation of the snapshot  $\underline{x}(t_\ell)$  with  $\ell$  taking values  $1, 2, \dots, N_p \mathcal{N}_c$  is updated by adding a second subscript  $n$ , i.e.  $\underline{x}(t_{n,\ell})$ , to indicate the  $\ell^{\text{th}}$  snapshot in the  $n^{\text{th}}$  PRI, with  $\ell$  now taking values  $1, 2, \dots, N_p \mathcal{N}_c$  and  $n = 1, 2, \dots, N_s$ . This snapshot can be modelled as:

$$\begin{aligned} \underline{x}(t_{n,\ell}) &= \underbrace{\sum_{k=1}^K \sqrt{P_{Tx}} \beta_k a[n] \exp(j2\pi \mathcal{F}_k \ell T_c) \bar{\mathbb{S}}_k^H \underline{\text{col}}_\ell \left[ (\mathbb{J}^{d_k} \mathbb{C}_{\text{ex}})^T \right] S_k}_{\text{scalar}_{k,n,\ell}} \\ &\quad + \underline{x}_c(t_{n,\ell}) + \underline{n}(t_{n,\ell}) \\ &= \sum_{k=1}^K \text{scalar}_{k,n,\ell} \cdot S_k + \underline{x}_c(t_{n,\ell}) + \underline{n}(t_{n,\ell}) \end{aligned} \quad (33)$$

where  $\underline{\text{col}}_\ell \left[ (\mathbb{J}^{d_k} \mathbb{C}_{\text{ex}})^T \right]$  denotes the  $\ell^{\text{th}}$  column of the matrix  $(\mathbb{J}^{d_k} \mathbb{C}_{\text{ex}})^T \in \mathcal{R}^{\bar{N} \times N_p \mathcal{N}_c}$

$$\begin{aligned} (\mathbb{J}^{d_k} \mathbb{C}_{\text{ex}})^T &= \begin{bmatrix} 0, & \cdots & 0, & \overbrace{\alpha_1[1], & \cdots & \alpha_1[\mathcal{N}_c],}^{\triangleq \mathbb{C}^T}, & 0, & \cdots & 0 \\ 0, & \cdots & 0, & \alpha_2[1], & \cdots & \alpha_2[\mathcal{N}_c], & 0, & \cdots & 0 \\ \vdots & & \vdots & & & & \vdots & & \vdots \\ 0, & \cdots & 0, & \alpha_{\bar{N}}[1], & \cdots & \alpha_{\bar{N}}[\mathcal{N}_c], & 0, & \cdots & 0 \end{bmatrix} \\ &\quad \begin{matrix} d_k \text{ columns} \\ \bar{N} \text{ zeros} \end{matrix} \quad \begin{matrix} \triangleq \mathbb{C}^T \\ \mathcal{N}_c - d_k \text{ columns} \\ \bar{N} \text{ zeros} \end{matrix} \end{aligned} \quad (34)$$

Note that the shifting matrix  $\mathbb{J} \in \mathcal{R}^{N_p \mathcal{N}_c \times N_p \mathcal{N}_c}$  is defined as

$$\mathbb{J} = \begin{bmatrix} 0_{N_p \mathcal{N}_c-1}^T, & 0 \\ \mathbb{I}_{N_p \mathcal{N}_c-1}, & 0_{N_p \mathcal{N}_c-1} \end{bmatrix}$$

and the operation of the  $\mathbb{J}^{d_k} \mathbb{C}_{\text{ex}}$  is down shifting the

columns of the code matrix  $\mathbb{C}_{ex}$  by  $d_k$  elements which is the amount of discrete delay  $d_k$  corresponding to the  $k$ -th target.

- the snapshots are assembled first into PRIs and then CPI interval, as shown in Figure 4a. The  $\ell$ <sup>th</sup> snapshot of the 1<sup>st</sup> PRI is also shown in Figure 4a as  $\underline{x}(t_{1,\ell})$ . Thus during an observation interval of  $N_p \mathcal{N}_c$  snapshots, corresponding to data matrix of the  $n$ <sup>th</sup> PRI  $\mathbb{X}[n] \in \mathcal{C}^{N \times N_p \mathcal{N}_c}$  can be modelled as follows:

$$\begin{aligned} \mathbb{X}[n] &= [\underline{x}(t_{n,1}), \dots, \underline{x}(t_{n,\ell}), \dots, \underline{x}(t_{n,N_p \mathcal{N}_c})] \\ &= \underbrace{\sum_{k=1}^K \sqrt{P_{Tx}} \beta_k a[n] \underline{S}_k \underline{S}_k^H}_{\text{(echoes from } K\text{-targets)}} \underbrace{\left( \begin{array}{c} \mathbb{J}^{d_k} \mathbb{C}_{ex} \\ \vdots \\ \mathbb{J}^{d_K} \mathbb{C}_{ex} \end{array} \right)^T \odot \left( \begin{array}{c} \mathbb{J}^{d_k} \mathbb{F}_{c,k} \\ \vdots \\ \mathbb{J}^{d_K} \mathbb{F}_{c,k} \end{array} \right)}_{\triangleq \mathbb{T}(d_k, \mathcal{F}_k)} \\ &\quad + \mathbb{X}_c[n] \quad \text{(clutter term)} \\ &\quad + \mathbb{N}[n] \quad \text{(noise term)} \end{aligned} \quad (35)$$

where

$$\underline{\mathcal{F}}_{c,k} \triangleq \exp \left( j2\pi \mathcal{F}_k \begin{bmatrix} 1 \\ 2 \\ \vdots \\ N_p \mathcal{N}_c \end{bmatrix} T_c \right) \in \mathcal{C}^{N_p \mathcal{N}_c \times 1} \quad (36)$$

$$\begin{aligned} \mathbb{X}_c[n] &= [\underline{x}_c(t_{n,1}), \dots, \underline{x}_c(t_{n,\ell}), \dots, \underline{x}_c(t_{n,N_p \mathcal{N}_c})] \\ \mathbb{N}[n] &= [\underline{n}(t_{n,1}), \dots, \underline{n}(t_{n,\ell}), \dots, \underline{n}(t_{n,N_p \mathcal{N}_c})] \end{aligned}$$

- Vectorisation of Equation 35 will provide the  $n$ <sup>th</sup> column (associated with  $n$ <sup>th</sup> PRI) of Figure 4b represented by the vector  $\underline{x}_{st}[n]$  which is modelled as follows:

$$\begin{aligned} \underline{x}_{st}[n] &= \text{vec}(\mathbb{X}^T[n]) \in \mathcal{C}^{N N_p \mathcal{N}_c \times 1} \\ &= \sum_{k=1}^K \sqrt{P_{Tx}} \beta_k a[n] \underbrace{\underline{S}_k \underline{S}_k^H}_{\text{scalar}} \underbrace{\left( \begin{array}{c} \mathbb{J}^{d_k} \underline{\mathcal{C}}_s \\ \vdots \\ \mathbb{J}^{d_K} \underline{\mathcal{C}}_s \end{array} \right)}_{\underline{h}_{st,k}} \end{aligned} \quad (37)$$

with the composite code vector  $\underline{\mathcal{C}}_s$  defined as the addition of all the  $\overline{N}$  PN-codes that is:

$$\underline{\mathcal{C}}_s \triangleq \mathbb{C}_{ex} \underline{1}_{\overline{N}} \in \mathcal{R}^{N_p \mathcal{N}_c \times 1} \quad (38)$$

- Finally the  $\text{vec}(\mathbb{X}^T[n])$  is projected as follows to provide one column of Figure 4c

$$\begin{aligned} \underline{x}_{vst}[n] &= \left[ \begin{array}{c} (\mathbb{I}_N \otimes \mathbb{P}_{\mathbb{B}_1}^\perp) \\ (\mathbb{I}_N \otimes \mathbb{P}_{\mathbb{B}_2}^\perp) \\ \vdots \\ (\mathbb{I}_N \otimes \mathbb{P}_{\mathbb{B}_m}^\perp) \\ \vdots \\ (\mathbb{I}_N \otimes \mathbb{P}_{\mathbb{B}_{\overline{N}}}^\perp) \end{array} \right] \underbrace{\text{vec}(\mathbb{X}^T[n])}_{\triangleq \underline{x}_{st}[n]} \end{aligned} \quad (39a)$$

$$= \sum_{k=1}^K \sqrt{P_{Tx}} \beta_k a[n] \mathbb{P}_{\mathbb{B}}^\perp \underline{h}_k + \underline{x}_{v,c}[n] + \underline{n}_v[n] \quad (39b)$$

where

$$\underline{h}_k \triangleq \underline{S}_k \otimes \underline{S}_k^* \otimes (\mathbb{J}^{d_k} \underline{\mathcal{C}}_s \odot \underline{\mathcal{F}}_{c,k}) \quad (40)$$

and  $\mathbb{P}_{\mathbb{B}_m}^\perp \in \mathcal{C}^{N_p \mathcal{N}_c \times N_p \mathcal{N}_c}$  is a complement subspace projection operator to isolate the signal from  $m$ -th Tx antenna from the rest and is defined as

$$\mathbb{P}_{\mathbb{B}_m}^\perp \triangleq \mathbb{I}_{N_p \mathcal{N}_c} - \mathbb{B}_m (\mathbb{B}_m^H \mathbb{B}_m)^{-1} \mathbb{B}_m^H \quad (41)$$

with

$$\mathbb{B}_m = \begin{bmatrix} \mathbb{J}^{d_1} \mathbb{C}_m \odot \left( \underline{\mathcal{F}}_{c,1} \underline{1}_{\overline{N}-1}^T \right) \\ \mathbb{J}^{d_2} \mathbb{C}_m \odot \left( \underline{\mathcal{F}}_{c,2} \underline{1}_{\overline{N}-1}^T \right) \\ \vdots \\ \mathbb{J}^{d_K} \mathbb{C}_m \odot \left( \underline{\mathcal{F}}_{c,K} \underline{1}_{\overline{N}-1}^T \right) \end{bmatrix}^T \quad (42)$$

note that the matrix  $\mathbb{B}_m \in \mathcal{C}^{N_p \mathcal{N}_c \times K(\overline{N}-1)}$  represents the part of extended array response vector covering delay and Doppler parameters for  $K$  targets. Where  $\mathbb{C}_m \in \mathcal{C}^{N_p \mathcal{N}_c \times (\overline{N}-1)}$  is the code matrix  $\mathbb{C}_{ex,m}$  with  $m$ -th antenna's code removed as shown below:

$$\mathbb{C}_m = [\underline{c}_1, \dots, \underline{c}_{m-1}, \underline{c}_{m+1}, \dots, \underline{c}_{\overline{N}}] \quad (43)$$

A similar projection operator matrix  $\mathbb{P}_{\mathbb{B}}^\perp \in \mathcal{C}^{N \overline{N} N_p \mathcal{N}_c \times N \overline{N} N_p \mathcal{N}_c}$  can be formed for every  $m$ , that is for all antennas, and the overall operator for the whole array can be represented as follow:

$$\mathbb{P}_{\mathbb{B}}^\perp = \begin{bmatrix} \mathbb{I}_N \otimes \mathbb{P}_{\mathbb{B}_1}^\perp, \mathbb{O}_{N N_p \mathcal{N}_c}, \dots, \mathbb{O}_{N N_p \mathcal{N}_c}, \\ \mathbb{O}_{N N_p \mathcal{N}_c}, \mathbb{I}_N \otimes \mathbb{P}_{\mathbb{B}_2}^\perp, \dots, \mathbb{O}_{N N_p \mathcal{N}_c}, \\ \vdots \quad \vdots \quad \ddots \quad \vdots \\ \mathbb{O}_{N N_p \mathcal{N}_c}, \mathbb{O}_{N N_p \mathcal{N}_c}, \dots, \mathbb{I}_N \otimes \mathbb{P}_{\mathbb{B}_{\overline{N}}}^\perp \end{bmatrix} \quad (44)$$

Equation 39b reveals that  $\underline{x}_{vst}[n]$  is a function of the extended array manifold vector  $\underline{h}_k \in \mathcal{C}^{N \overline{N} N_p \mathcal{N}_c \times 1}$

### B. Joint Range and Doppler Estimation

First, the range =  $d_k T_c c$  and the Doppler  $\mathcal{F}_k \forall k$ , can be estimated using the following cost function:

$$(\underline{d}, \underline{\mathcal{F}}) = \arg \max_{d, \mathcal{F}} \xi(d, \mathcal{F}), \forall d, \mathcal{F} \quad (45)$$

where

$$\xi(d, \mathcal{F}) = \frac{\det(\mathbb{T}(d, \mathcal{F})^H \mathbb{T}(d, \mathcal{F}))}{\det(\mathbb{T}(d, \mathcal{F})^H \mathbb{P}_n \mathbb{T}(d, \mathcal{F}))}, \forall d, \mathcal{F} \quad (46)$$

with

$$\mathbb{T}(d, \mathcal{F}) = \mathbb{J}^d \mathbb{C}_{ex} \odot (\underline{1}_{\overline{N}} \underline{\mathcal{F}}_c) \quad (47)$$

$\mathbb{T}(d, \mathcal{F})$  is the transformation matrix defined in Equation 35. Furthermore, the matrix  $P_n$  in Equation 46, is the projection operator to the noise subspace, spanned by the "noise" eigenvalues of the data covariance matrix

$$\mathbb{R}_{\mathbb{X}\mathbb{X}} = \frac{1}{N \cdot N_s} \sum_{n=1}^{N_s} \mathbb{X}[n] \mathbb{X}[n]^H \quad (48)$$

### C. Joint DOA and DOD Estimation

Using the above-estimated delay and Doppler the complement projection operator  $\mathbb{P}_{\mathbb{B}}^\perp$  can be constructed to form the

TABLE I: System Parameters

Parameter	Value	Comment
$F_c$	1.3GHz	RF Carrier Frequency
$T_c, T_s$	$T_s = T_c$	Chip interval = Sampling frequency
$B$	$\frac{1}{T_c}$	RF bandwidth
$\bar{N}, N$	5	Tx and Rx UCAs elements
Rx SNR	20dB	Rx Signal to Noise Ratio
$\mathcal{N}_c$	15	PN-code length/period
$T_p$	$T_c \mathcal{N}_c$	Pulse duration
$R_u$	262	Unambiguous range (in units of compressed range bins)
PRI	$2R_u T_c$	Pulse Repetition Interval
PRF	$\frac{1}{\text{PRI}}$	Pulse Repetition Frequency
$L$	$\frac{\text{PRI}}{T_c}$	Compressed Range bins per PRI
$N_s$	256	Number of PRIs per CPI

virtual spatiotemporal snapshot vector  $\underline{x}_{\text{vst}}[n]$ . This enables to estimate the DOA and DOD using the cost function below:

$$(\underline{\theta}, \bar{\theta}) = \arg \max_{\forall(\theta, \bar{\theta})} \xi(\theta, \bar{\theta})|_{d=d_k, \mathcal{F}=\mathcal{F}_k}, \forall \theta, \bar{\theta} \quad (49)$$

and  $\xi(\theta, \bar{\theta})$  can be defined as below:

$$\xi(\theta, \bar{\theta}) \triangleq \sum_{k=1}^K \left( \frac{\|\mathbb{P}_{\mathbb{B}}^{\perp} h_k(\theta, \bar{\theta})\|^2}{(\mathbb{P}_{\mathbb{B}}^{\perp} h_k(\theta, \bar{\theta})) \mathbb{P}_{\text{nv}} (\mathbb{P}_{\mathbb{B}}^{\perp} h_k(\theta, \bar{\theta}))} \right), \forall \theta, \forall \bar{\theta} \quad (50)$$

where  $\mathbb{P}_{\text{nv}}$  is the projection operator to the noise subspace spanned by the "noise" eigenvector of the covariance matrix of the virtual-spatiotemporal snapshots given by Equation 39a

$$R_{xx} = \frac{1}{N_s} \sum_{n=1}^{N_s} \underline{x}_{\text{vst}}[n] \underline{x}_{\text{vst}}[n]^H \quad (51)$$

## V. COMPUTER SIMULATIONS

In this section the performance of the proposed approach is examined using computer simulation studies. Table I lists the system's parameters. The RF carrier frequency is set to 1.3 GHz for this simulation. The DAC and ADC sampling interval  $T_s$  is equal to  $T_c$  and the unambiguous range  $R_u$  is assumed to be 262 compressed range bins while the PRI is  $2R_u T_c$ . The PN-code length/period  $\mathcal{N}_c = 15$  for pulse compression is also assumed.

As shown in Figure 5, both the radar's Tx and Rx use uniform circular arrays (UCA). The Rx antenna array elements are separated by a distance  $d = \frac{\lambda}{2}$  while the Tx elements are separated by  $3d$  and each element has a unity gain ( $G_{Tx} = G_{Rx} = 1$ ). Equations 52 and 53 provide the Tx and Rx antenna array geometries (Cartesian coordinates) on a 3-D real space in meters. The Tx and Rx arrays or sites are separated by  $L_{bi} = 95$  units of compressed range bins.

All antenna array elements are along the x and y-axis and no element is across the z-axis.

$$\begin{aligned} \underline{\mathbf{r}} &= [\underline{r}_1, \underline{r}_2, \dots, \underline{r}_N] \\ &= \begin{bmatrix} 0.28, & 0.09, & -0.22, & -0.22, & 0.09 \\ 0, & 0.26, & 0.16, & -0.16, & -0.26 \\ 0, & 0, & 0, & 0, & 0 \end{bmatrix} \end{aligned} \quad (52)$$

$$\begin{aligned} \underline{\mathbf{r}} &= [r_1, r_2, \dots, r_N] \\ &= \begin{bmatrix} 0.092, & 0.028, & -0.074, & -0.074, & 0.028 \\ 0, & 0.087, & 0.054, & -0.054, & -0.087 \\ 0, & 0, & 0, & 0, & 0 \end{bmatrix} \end{aligned} \quad (53)$$

where  $d$  is defined as:

$$d = \frac{\lambda}{2} = \frac{c}{2F_c}$$

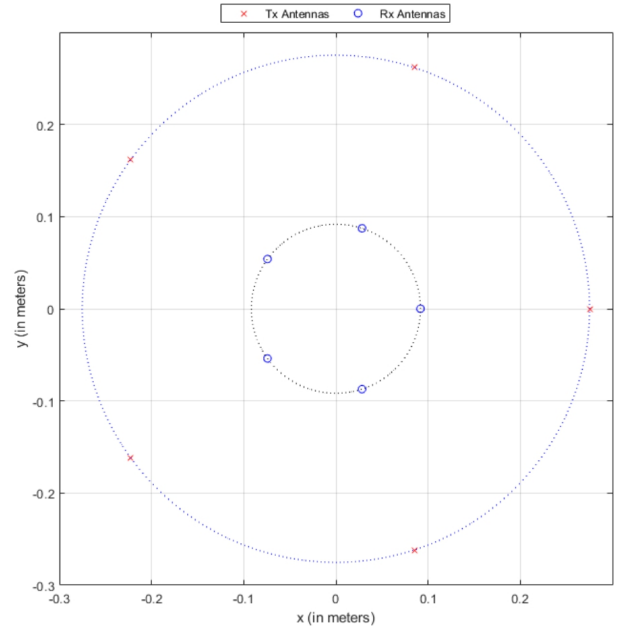


Fig. 5: Tx and Rx UCA

Figure 5 shows both antenna arrays with reference to their own local reference points. The figure does not show the distance between the Tx and Rx array. Figure 6 shows a bistatic radar system with Tx and Rx Cartesian coordinate location and three targets on the (x,y) plane. The elevation angle is assumed zero.

Table II summarises the geometric parameters of three targets along with their RCS model and average values. From this table, RCS values in conjunction with the Swerling probability density functions, are used to generate the received reflections (random numbers) for each target.

As described in Section 2, the transmitted waveform with PN-codes (either m-code or Gold codes) for pulse compression provides orthogonality within a PRI period. The period could be adjusted for required target illumination and the resulting signal-to-noise ratio.

TABLE II: Targets Parameters

Parameter	Target-1	Target-2	Target-3	Comments
$R_{Tx}$	51	85	126	Tx to Target range (in compressed range bins)
$R_{Rx}$	101	104	102	Rx to Target range (in compressed range bins)
$R_{bi}$	152	189	228	Bistatic range = $R_{Tx} + R_{Rx}$ (in compressed range bins)
$\theta$	150°	130°	100°	Direction of Arrival (DOA)
$\bar{\theta}$	81.20°	70.83°	52.31°	Direction of Departure(DOD)
$\zeta$	68.80°	59.17°	47.69°	Bistatic Angle
RCS	$1.0 \text{ m}^2$	$1.5 \text{ m}^2$	$2 \text{ m}^2$	Radar Cross-Section
Swerling Model	1 <sup>st</sup> model	2 <sup>nd</sup> model	3 <sup>rd</sup> model	Swerling model for RCS
$v$	-60 m/sec	20 m/sec	60 m/sec	Radial Velocity

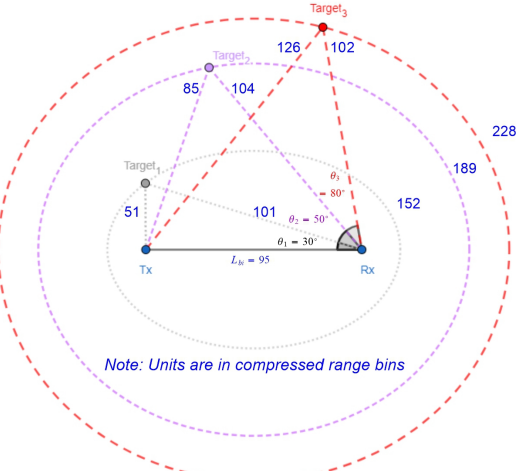


Fig. 6: Targets' Geometry

The radar also is assumed to operate in the presence of ground clutter and AWGN. The ground clutter can be modelled using various other PDFs such as K-distribution and Weibull etc. It is often challenging to model and filter various types of clutters accurately because different objects/terrains cannot be represented by a single model. One effective approach is to transform the clutter PDFs to Gaussian i.e. transform the coloured clutter to white noise (isotropic) and then filter it out the same way as white noise [12]. The clutter filtering for this experiment is implemented as described in [12].

#### A. Range and Doppler Estimation

The range and Doppler can be estimated jointly by just utilising temporal dimension of the data and array manifold. Therefore, the cost function of Equation 46 is used for the estimation. Figure 7 shows that the peaks are sharp and the estimates are very close to the range and Doppler resolution error. The results are summarised in Table III below.

#### B. DOA and DOD Estimation

A joint DOA and DOD estimation is performed using the cost function of Equation 50. As shown in Figure 8 and Table IV below, the estimates are very close.

TABLE III: Bistatic Range and Doppler Estimations

Target	$R_{bi}(T_c)$		Doppler (Hz)	
	True	Estimated	True	Estimated
1	152	152	-429.37	-428.37
2	189	189	150.84	151.13
3	228	228	475.94	475.13

TABLE IV: DOA and DOD Estimation

Target	$\bar{\theta}$		$\theta$	
	True	Estimated	True	Estimated
1	81.20°	81.20°	150.00°	150.01°
2	70.83°	70.83°	130.00°	130.01°
3	52.31°	52.31°	100.00°	100.02°

#### C. RMSE and Comparison

The algorithm, as denoted by Equation 50, has been rigorously assessed utilizing Monte Carlo simulations and the Root Mean Square Error (RMSE) method. A comparative analysis has been conducted against the standard bistatic radar estimation method, given in Appendix A. The error assessment for the parameter of interest  $p$  is defined as per the following equation:

$$RMSE_p = \frac{1}{K} \sum_{k=1}^K \sqrt{\mathcal{E}\{|\hat{p}_k - p_k|^2\}} \quad (54)$$

Where  $p_k$  represents the general parameter of interest for the  $k$ -th target.

The comparison depicted in Figure 9 is annotated with subscript letters corresponding to the DOD and DOA values in the legend, represented as follows:

- DOD<sub>v-ST</sub>: DOD with v-ST algorithm.
- DOA<sub>v-ST</sub>: DOA with v-ST algorithm.
- DOD<sub>m</sub>: DOD with MUSIC algorithm and bistatic geometry.
- DOA<sub>m</sub>: DOA with MUSIC algorithm.

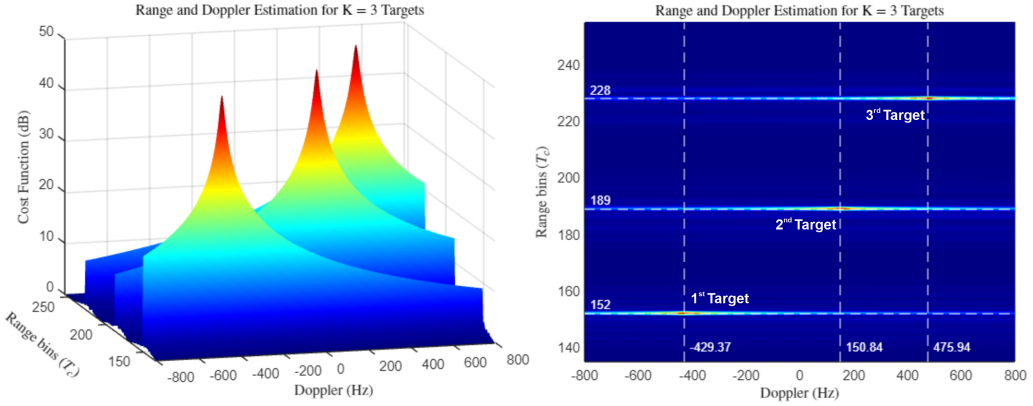


Fig. 7: Range and Doppler Estimation.

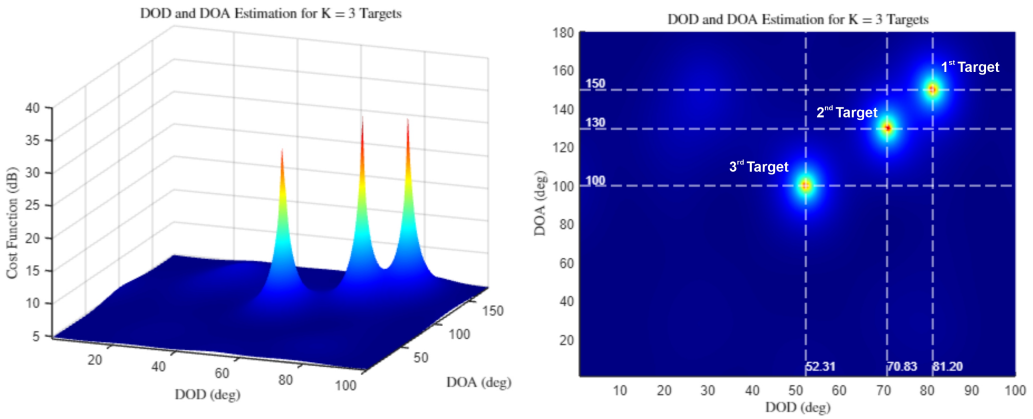


Fig. 8: DOA and DOD Estimation.

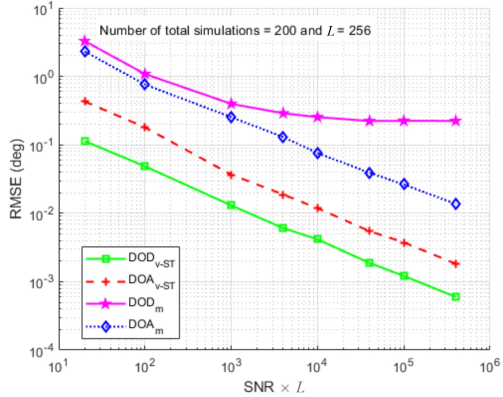


Fig. 9: DOA and DOD RMSE

The performance depicted in the figure demonstrates the superior efficacy of the proposed virtual Spatiotemporal (v-ST) algorithm when compared to conventional bistatic estimation techniques. It is noteworthy that the  $DOD_m$  exhibits a floor-level trend beyond the mid-trace, attributable to range floor-level quantization error limitations.

## CONCLUSIONS

In conclusion, this paper investigated the application of novel subspace algorithms for parameter estimation in MIMO

bistatic pulse radar systems. The proposed approach uses a unique PN-code for each transmit chain, maximising the observation space by utilizing both the Tx and Rx observation spaces. The channel model incorporates  $K$  moving targets with Swerling-distributed RCS and accounts for clutter and noise. The received signal model is constructed, and a 3D radar data cube is assembled. This data undergoes processing through Spatiotemporal and Virtual Spatiotemporal manifold extenders to increase the degree of freedom and improved parameter estimation.

Computer simulations were conducted to evaluate the performance of the proposed direction-of-arrival (DOA) and direction-of-departure (DOD) estimation algorithm. Using Monte Carlo simulations and Root Mean Square Error (RMSE) as a metric, a comparison with the bistatic MIMO radar equations in conjunction with the MUSIC algorithm revealed the superior performance of the proposed system.

## ACKNOWLEDGMENTS

This research would not have been possible without the funding from Saab Research Sweden/UK. The authors, in particular, would also like to express their deepest gratitude to Prof. Anders Silander (Saab) and Malin Svahn (Saab, VP Director of Innovation Programmes) for their continuous support and encouragement.

## REFERENCES

- [1] M. A. Richards, J. A. Scheer, and W. A. Holm, *Principles of Modern Radar: Basic Principles*. Institution of Engineering and Technology, Jan 2010.
- [2] W. L. Melvin and J. A. Scheer, "Principles of Modern Radar: Advanced Techniques," *Principles of Modern Radar: Advanced Techniques*, pp. 1–846, Jan 2013.
- [3] K. Luo and A. Manikas, "Superresolution Multitarget Parameter Estimation in MIMO Radar," *IEEE Transactions on Geoscience and Remote Sensing*, vol. 51, no. 6, pp. 3683–3693, 2013.
- [4] M. Laid Bencheikh, Y. Wang, and H. He, "A Subspace-based Technique for Joint DOA-DOD Estimation in Bistatic MIMO Radar," in *4th Microwave and Radar Week MRW-2010 - 11th International Radar Symposium, IRS 2010 - Conference Proceedings*, 2010, pp. 170–173.
- [5] F. Wen, J. Shi, and Z. Zhang, "Joint 2D-DOD, 2D-DOA, and Polarization Angles Estimation for Bistatic EMVS-MIMO Radar via PARAFAC Analysis," *IEEE Transactions on Vehicular Technology*, vol. 69, no. 2, pp. 1626–1638, Feb 2020.
- [6] C. Cui, J. Xu, R. Gui, W. Q. Wang, and W. Wu, "Search-Free DOD, DOA and Range Estimation for Bistatic FDA-MIMO Radar," *IEEE Access*, vol. 6, pp. 15 431–15 445, Mar 2018.
- [7] A. Sakhnini, A. Bourdoux, and S. Pollin, "Bistatic mimo radar with unsynchronized arrays," in *2023 IEEE Radar Conference (RadarConf23)*, Jun 2023, pp. 1–5.
- [8] A. Manikas, *Differential Geometry in Array Processing*. London, U.K.: Imperial College Press, Aug 2004.
- [9] G. Efthathopoulos and A. Manikas, "Extended Array Manifolds: Functions of Array Manifolds," *IEEE Transactions on Signal Processing*, vol. 59, no. 7, pp. 3272–3287, Jul 2011.
- [10] Z. Tang and A. Manikas, "DOD-DOA Estimation using MIMO Antenna Arrays with Manifold Extenders," *2022 IEEE 33rd Annual International Symposium on Personal, Indoor and Mobile Radio Communications (PIMRC)*, pp. 535–540, Sep 2022.
- [11] H. Commin and A. Manikas, "Virtual SIMO Radar Modelling in Arrayed MIMO Radar," in *Sensor Signal Processing for Defence (SSPD 2012)*. IET, 2012, pp. 1–6.
- [12] H. Ren and A. Manikas, "MIMO Radar with Array Manifold Extenders," *IEEE Transactions on Aerospace and Electronic Systems*, vol. 56, no. 3, pp. 1942–1954, Dec 2020.

## APPENDIX

## A. Bistatic Estimation Process

- 1) Compute the bistatic range estimation ( $R_{bi}$ ) using Equation 46.
- 2) Using  $L_{bi}$  and  $R_{bi}$ , determine the following bistatic target's ellipse parameters:
  - semi-major axis  $a$
  - semi-minor axis  $b$ , and
  - its eccentricity  $\varepsilon$ ,  
using Equations 57-59 of Appendix B.
- 3) Calculate the Tx to Target Range ( $R_{Tx}$ ) and Target to Rx Range ( $R_{Rx}$ ) using Equations 60 and 61 of Appendix B.
- 4) Using the MUSIC algorithm estimate the Direction of Arrival (DOA<sub>m</sub>).
- 5) Estimate the Direction of Departure (DOD<sub>m</sub>) using Equation 62 given in Appendix B

## B. Bistatic Equations

The estimated target delay parameters  $d_k$  can be converted to bistatic range  $R_{bi}$  as follows.

$$R_{bi,k} = d.c.T_c |_{d=d_k}, \forall k \quad (55)$$

$$R_{bi,k} = R_{Tx,k} + R_{Rx,k} \quad (56)$$

With reference to Figure 10 which shows a bistatic ellipse and its parameters, the values  $R_{bi,k}$  and  $L_{bi}$  can be used to estimate the parameters  $a_k$ ,  $b_k$  and  $\varepsilon_k$  as follows:

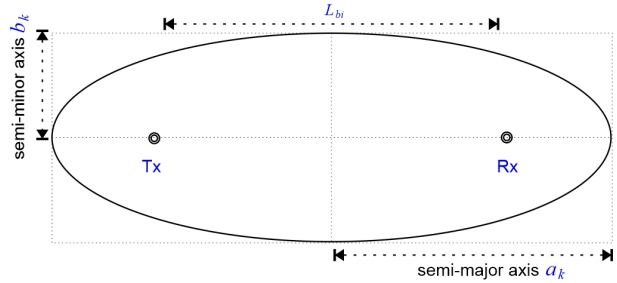


Fig. 10: Ellipse notations

$$\text{semi-major axis } a_k = \frac{R_{bi,k}}{2}, \forall k \quad (57)$$

$$\text{semi-minor axis } b_k = \sqrt{R_{bi,k}^2 - \frac{L_{bi}^2}{4}} \quad (58)$$

$$\text{eccentricity ratio } \varepsilon_k = \frac{L_{bi}/2}{a_k} \quad (59)$$

Furthermore, the bistatic ranges  $R_{Rx}$  (Target to Rx) and  $R_{Tx}$  (Tx to Target) for each target can be estimated using the following equations:

$$R_{Rx,k} = \frac{a_k(\varepsilon_k^2 - 1)}{\varepsilon_k \cos(\theta_k) + 1}, \forall k \quad (60)$$

$$R_{Tx,k} = R_{bi,k} - R_{Rx,k} \quad (61)$$

Finally, using the above equation, the DOD  $\bar{\theta}_k$   $\forall k$  can be estimated as follow:

$$\bar{\theta}_k = \arccos \left( \frac{1}{\varepsilon_k} \left( \frac{a_k(\varepsilon_k^2 - 1)}{R_{Tx,k}} + 1 \right) \right) \quad (62)$$



**Nadeem Dar** received his BEng (Honours) degree in Communication Systems Engineering from the University of Westminster, London, in 2000 and his MSc degree in Electronic and Electrical Engineering from Anglia Ruskin University, Cambridge, in 2019. Currently, he is pursuing his PhD degree within the Communications and Signal Processing Group at Imperial College London's Department of Electrical and Electronic Engineering. His research focuses on advanced topics in bistatic/multistatic arrayed MIMO radar systems, with a particular emphasis on array signal processing, super-resolution parameter estimation, and space-time array processing.



**Athanassios Manikas**, please see:  
<https://skynet.ee.ic.ac.uk/manikas.html>